

# Oscillations Damping and Stability Improvement of Solar Photo-Voltaic Cell and Battery Energy Storage System Connected to a D.C. Microgrid using Metaheuristic Optimized PID Controller

Mohamed M.H. Adam\*, Ameer Naeem, Nabil Hidayat, Noor Fadzilah Mohamed Shariff, V., Naeem M.S. Hannon and Vijayakumar Varadarajan

**Abstract**— DC micro-grid is most preferred now a day for Renewable energy sources such as solar, wind, and bio-diesel to share electrical power. At large, a solar photovoltaic (PV) electric power production is supported by a battery energy storage system (BESS) for continuous and reliability of power supply to the loads. To extract maximum power from the solar or wind renewable source, Maximum Power Point Tracking (MPPT) with dc-to-dc voltage control plays a vital role. In this paper, early synchronizing and MPPT of solar power to the grid and better active power transfer capability is analyzed. For this, Metaheuristic Optimization based Proportional Integral and Derivative (MOPID) controllers like Whale Optimization Algorithm (WOA) and Grey-Wolf Optimization (GWO) algorithms are compared to show the effectiveness of the operation. These controllers are used in the control scheme of the solar MPPT dc-dc converter operation have better damping and power transferrable capability with earlier settling time and overshoot compared to a system without a controller. The performance of the system is verified through MATLAB/ Simulink simple dc-microgrid environment

**Index Terms**—Solar photovoltaic (PV), microgrid (MG), power oscillations damping, BESS, adaptive fuzzy proportional integral and derivative (FPID) controller.

## I. INTRODUCTION

WITH the rapid advancements and research in power electronics and renewable energy resources, solar photovoltaic (PV) cell interest is increasing at a very high pace [1]. This solar PV cell is used in all developing and developed countries with the scope of use in the meager rating of few watts to megawatts application like toys, electronic boards, lighting, traffic control systems, electric vehicle charging and for power generation to nearby industrial loads of a few MWs [2].

This manuscript is submitted on 10<sup>th</sup> November 2022 and accepted on 4<sup>th</sup> October 2023. Mohamed Mohmaed Adam, Assoc. Prof Dr. Muhamad Nabil Hidayat and Associate Prof Dr. Naeem Hannon are from the College of Engineering, Universiti Teknologi MARA. 40450 Shah Alam, Selangor. Ammer bin Naeem and Noor Fadzilah bt Mohamed Shariff are from Universiti Pertahanan Malaysia. V. and Prof Vijayakumar Varadarajan from Ajeenkya D Y Patil University India.

\*Corresponding author  
Email address: mohamedsolar7781@gmail.com

1985-5389/© 2023 The Authors. Published by UiTM Press. This is an open access article under the CC BY-NC-ND license (<http://creativecommons.org/licenses/by-nc-nd/4.0/>)

Since the PV cell is dc and the grid and loads are generally AC, it requires at least one stage conversion [3]. For higher power handling and raid control, mostly multi-stage is very famous and used for a long time [4-6]. Recently, single-stage solar PV inverter topologies are recognized for low power direct grid or smaller rating load applications.

There is a considerable interest in installing renewable energy resources, especially in solar and wind-based electrical power generation observed globally. Based on global wind energy organization statistics, China, the U.S.A., and India are the three top countries in the world, it has been completed generating more than 10,000 MW of solar power by march 2018 [7]. China is producing 43.5 GW in 2015, while it increased to 78 GW, 131 GW, and 175 GW in 2016, 17, and 2018 years respectively, with a growth of 3%. Similarly, the German growth rate by the end of 2018 is 7.9%, Italy 7.3%, Japan 6.8%, and India it is 5.4% [8]. Many countries are spending about 2.5% of their total budget towards renewable and especially half of this is for solar energy for the last five years and is increasing in budget rate year by year. The absolute solar power installed by European countries alone installed 98.8GW, Asia 92.3, East Asia with 79.5GW, North America 29.8 GW and remaining continents around 50GW with the global installation of almost 323.73 GW in 2016. India alone producing about 9200 MW in 2017, and 9600 MW generation is in progress during the same year and targeted more than 175 GW by this 2023.

The DC microgrid for solar PV system with particle swarm optimization (PSO) and Perturb & Observe (P&O) maximum power point tracking (MPPT) . MPPT algorithm in real-time environment with improved stability and quicker dynamic response [9]. The solar PV with DC microgrid coupled inductor SEPIC converter using fuzzy logic controller (FLC) to improve the efficiency of power on microgrid [10]. The PV and Fuel Cell through DC-DC boost converters fuzzy (FLC) MPPT to reduce steady-state oscillations and found that FLC is two times faster than neural network controllers and eighteen times faster than for PSO [11]. Solar PV BESS dc microgrid bus voltage variations and oscillations because of irregular irradiance variations and transient in loads are studied to increase BESS life time and higher current drawings [12]. A solar PV BESS with bi-directional converter for a standalone low voltage DC microgrid using dual loop PI based single control algorithm for effective voltage control and economic MPPT technique [13].

Improved Real Coded Genetic Algorithms is used to identify, trace and differentiate amid the open and short circuit faults in solar PV network [14]. An Artificial Neural Network with optimization-based global artificial gorilla troops MPPT metaheuristic approach to guarantee a reliable and operative MPPT abstraction [15]. An interesting quantum concept gravitational search particle swarm optimization (PSO) technique is compared with other algorithms to solve the economic load and emission dispatch for solar PV system [16]. A comprehensive review paper on parameter mining and fault recognition for solar PV cells using various metaheuristic techniques [17] to aid the upcoming researchers to attain precise, effective and quick fault detection. Partial shading effect of solar PV with GWO, MFO, PSO-GSA, SSA and Hybrid PSO-GSA metaheuristic optimization algorithms and found that GWO has quick convergence rate and better MPPT among all individual techniques [18]. Finally, this paper studies about stability, and better efficiency also with PSO-GSA and found that the hybrid methods are most effective, but little complicated. In [19], water cycle algorithm and moth-flame metaheuristic algorithms are used to solve techno- economic features due to renewables intermittencies.

A passivity method-based voltage regulation for a battery-supported solar PV system connected to dc M.G is used to obtain a transient response and stability analysis [20, 21]. Sepic converter-based solar PV, rectifier, buck converter-based wind PMSG and a bidirectional B.E.S system connected to a dc M.G topology are used for load management [22]. With a Hybrid energy storage system, (D.E.R) for a dc M.G was discussed with hardware-in-loop (H.I.L) [23], experimental evaluation for the solar PV, battery, and fuel cell for a dc M.G power management [24]. Solar PV with energy storage devices connected to a dc M.G

with droop voltage control characteristics for quicker vehicle charging application [25], another drooping control schemes discussed for a hybrid PV/hydrogen/battery DC MG for power management [26, 27], with combined P.I and sliding mode control technique (CPISMC) [28], with frequency filtering KDTFT [29] and Nonlinear integral back-stepping-based control [30]. Adaptive fuzzy and fuzzy P.I.D. Control methods are applied for dc M.G systems for current adaptive sharing [31], economic dispatch [32], and droop control for optimized power-sharing [33, 34].

In this paper, Grey-Wolf Optimization (GWO) and Whale Algorithm Optimization (WAO) for PID controllers are compared to find the effective controller for better synchronizing and active power extraction. So, solar PV, voltage, current, micro-turbines synchronous generator, and BESS parameters are verified. The solar PV cell-based dc-dc chopper connected to the dc microgrid to meet the fundamental features:

- i. To work effectively at the Maximum Power Point Tracking (MPPT) of the PV cells.
- ii. To function above the entire MPPT array of the PV cells.
- iii. To comprise a power rating corresponding to the maximum rating of PV cells.
- iv. Endure PV cell highest voltage and current rating despite the disparity in ambient temperature.
- v. Better performance to cost ratio compared to weight and size for residential rooftop installations.

- vi. Better reliability to compete with that of PV panels.
- vii. Improved efficiency.

However, with these advantages, few challenges need to overcome for better performance of solar-PV cell inverter :

- i. They constrained power handling capability.
- ii. Power output characteristics are vastly varying in nature.
- iii. Range of operation constrained due to imposed dc source.
- iv. With an increase in power handling capability, the price of the inverter set increases considerably.
- v. An increase in power handling capability resulting in high peak current stress
- vi. Few MPPT techniques are applicable as there is no intermediate chopper circuit.

Based on these disadvantages, the interest towards better and simple MPPT chopper design increases by compromising many switches, efficiency, and weight compared to a standard microgrid connection. Suppose these challenges are met to a certain extent. In that case, there can be a significant advance in the solar PV, topology applicable to rooftop household applications, hybrid electric vehicles, and other applications.

In section 2, the solar PV, grid-tied test-bed system is described. Solar PV, two area test-bed system discussed in section 3 and in section 4, famous metaheuristic algorithms along with WAO and GWO application metaheuristic algorithms pseudo-codes are discussed. Section 5 describes the simulation results with GWO and WAO in the MATLAB environment. The conclusion of the work is given in section 6.

## II. D.C. MICROGRID CONNECTED SOLAR P.V. BATTERY ENERGY STORAGE SYSTEM

In this section, modeling of solar PV, panel with battery energy storage system (BESS) connected to a common dc microgrid (M.G) and dc load is discussed analytically. Later block diagram representation of dc M.G solar PV, system is described mathematically. The dc M.G with subsystem components, switching design, dynamic current and voltage equations, and P.I controller-based output voltage equation is derived. In the block diagram representation, P.I controller modeling, solar PV, cell with MPPT controller, and buck-boost converter operation based on transfer function modeling are discussed.

### A. Modeling of dc microgrid based solar PV BESS system

In general, a solar photovoltaic (PV) electrical power generation system is supported with a battery energy storage system (BESS) for continuous and reliability of the power supply. This solar PV system is connected to ac or dc or hybrid AC/DC MG.

A solar PV dc M.G. system topology along with dc load is shown in Fig.1. This topology consists of subsystems like solar PV panel, solar MPPT boost converter, battery bank, bi-directional dc to dc converter connected to a common dc link terminal, buck converter for load connection. The solar PV panel consists of a current source with series and parallel resistances forming layers in the cell panel. This cell produces constant current and variable voltage depending on irradiation, temperature, shading, and other input factors. To extract continuous voltage from the solar PV cell with consistent D.C output, the maximum power point tracking (MPPT)

technique with dc voltage stepping up and to extract maximum power from the solar panel subsystem is beneficial [20-24]. The input voltage is  $V_1$ , and current  $i_1$  is given to the solar MPPT cell and is boosted using a designed inductor, switch, and a diode.

The switch  $S_1$  is having a duty cycle of  $d_1$ , the current through the MPPT diode  $D_3$  is  $i_2$ , and the output voltage of  $V_2$  from the MPPT subsystem produces constant voltage if input parameters are stable. This voltage is equal to the dc M.G voltage. A battery bank (BESS) with voltage  $E$  and internal resistance is in the figure supporting energy storage and retrieving when solar PV cells cannot supply power to the M.G and the load. The BESS is connected to the dc M.G using a bidirectional dc to dc converter with two switches numbered  $S_3$  and  $S_4$  with duty cycle  $d_2$ . If solar power output is sufficient, the battery gets charged, else it will supply power by discharging it based on the load and grid requirement. The output from the dc M.G is connected to the load using a buck step-down converter with the operation supported by switch  $S_2$  with duty cycle  $d_3$ , inductor  $L_3$ , and diode  $D_4$ . The output from the buck load converter is  $V_3$  which is the voltage across the capacitor  $C_2$  and is supplied to the load R.L. The voltages and currents dynamic equations are represented.

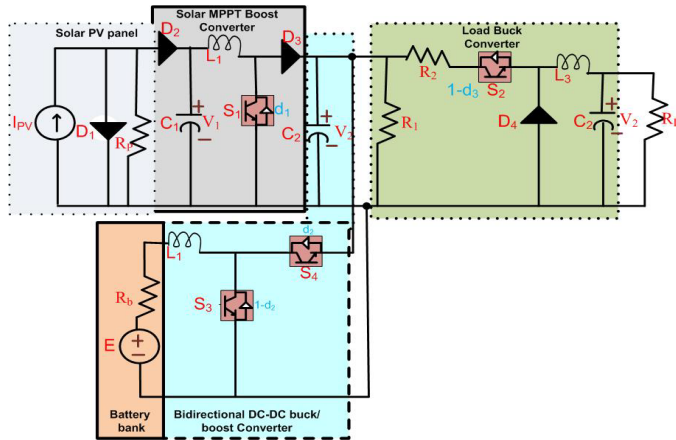


Fig.1. Solar PV BESS system connected to a dc microgrid

The input solar PV dynamic current flow is given by the equation (1)

$$L_1 \frac{di_1}{dt} = V_1 - V_2(1 - d_1) \quad (1)$$

Kirchoff's current and voltage equations are used for deriving each subsystem's voltage and current. Here,  $V_1$  is solar PV voltage, and  $V_2$  is M.G voltage with duty cycle  $d_1$  at switch  $S_1$  at solar MPPT boost converter [20, 21]. The battery energy storage system (BESS) dynamic current flow is given by equation (2). Here, the battery voltage is  $E$ , BESS current  $i_2$  with internal battery resistance  $R_b$  and the switch  $S_3$  at the bidirectional dc-dc buck-boost charging controller converter with duty cycle  $d_2$ .

$$L_2 \frac{di_2}{dt} = E - i_2 R_b - V_2 d_2 \quad (2)$$

The load current  $i_3$  flows through the load resistance R.L and switching operation controlling the buck voltage using the

switch  $S_2$  with duty cycle  $d_3$ , and the load voltage  $V_3$  is represented by the equation (3).

$$L_3 \frac{di_3}{dt} = (V_2 - i_3(1 - d_3)R_L)(1 - d_3) - V_3 \quad (3)$$

The solar PV cell output capacitor  $C_1$  dynamic voltage equation  $V_1$  is represented (4). This voltage is the difference between the source PV current and the boost converter current  $i_1$ . The solar PV current  $i_{pv}$ , diode current  $i_D$ . The diode voltage constant is 'a'.

$$C_1 \frac{dV_1}{dt} = i_s - i_1 = i_{pv} - i_D(e^{aV_1} - 1) - \frac{V_1}{R_p} - i_1 \quad (4)$$

The M.G voltage dynamic equation is given by all the switches duty cycles, and the M.G voltage is provided by the equation (5). Based on controlling the IGBT switches, voltage buck or boost operation is done, or in other terms, the dc M.G voltage is controlled using the switches duty cycles  $d_1$ ,  $d_2$  and  $d_3$ .

$$C_2 \frac{dV_2}{dt} = i_1(1 - d_1) + i_2 d_2 - i_3(1 - d_3) - \frac{V_2}{R_1} \quad (5)$$

The dc M.G dynamic load voltage  $V_3$  equation is represented using the equation (6).

$$C_3 \frac{dV_3}{dt} = i_3 - \frac{V_3}{R_2} \quad (6)$$

The solar PV output regulated voltage capacitor  $C_1$  value based on a common base capacitance value is given by equation (7). Here, the PV capacitor voltage value is taken one-fifth times its base value-based.

$$C_1 = \frac{0.01}{0.05C_b} \quad (7)$$

If the filter capacitor, power factor variation of the M.G is tacit within the limits of 5%. The maximum ripple current in the inductor  $L_1$  with switching time constant  $T_{sw}$  is given by the equation (8)

$$\Delta I_{L1max} = \frac{2V_{dc}}{3L_1}(1 - d_1)d_1 T_{sw} \quad (8)$$

The same inductor ripple current represented in terms of switching frequency  $F_{sw}$  instead of switching time constant is shown in equation (9) and if the PV IGBT switch  $d_1$  is considered as 0.5.

$$\Delta I_{L1max} = \frac{V_{dc}}{6F_{sw}L_1} \quad (9)$$

To obtain the maximum ripple from the panel MPPT output, if 10% ripple of rated current is considered, then the maximum ripple current is given by the equation (10),

$$\Delta I_{L1max} = 0.1I_{max} \quad (10)$$

Further, the maximum current output from the solar PV panel is given by the equation (11) represented in the form of solar PV real power PPV and solar PV input voltage  $V_{pv}$  (which is also equal to  $V_1$ )

$$I_{max} = \frac{\sqrt{2}P_{pv}}{3V_{pv}} \quad (11)$$

To reduce the current ripple to 20% with an attenuation factor  $K_a$ , the inductor MPPT  $L_1$  and battery-MG inductor  $L_2$  values can be represented using the equations (12) and (13)

$$L_1 = \frac{V_{dc}}{6F_{sw}\Delta I_{L1max}} \quad (12)$$

$$L_2 = \frac{1 + \frac{1}{\sqrt{K_a^2}}}{C_2\omega_{sw}^2} \quad (13)$$

To prevent the resonant conditions,  $R_1$  and  $R_2$  are helpful. They are also responsible for the reduction of ripple on switching frequency. Hence, the resistor  $R_1$  can be represented in terms of angular resonance frequency ( $\omega_{res}$ , rad/sec) is shown in equation (14)

$$R_1 = \frac{1}{3C_2\omega_{res}} \quad (14)$$

Where the angular resonance frequency ( $\omega_{res}$ ) is given by the equation (15)

$$\omega_{res} = \sqrt{\frac{L_1 + L_2}{L_1L_2C_2}} \quad (15)$$

The final bus voltage is given by vectorially all the subsystems voltages given by the equation (16)

$$V_2 = V_{20} + \frac{1}{C_2} \int_0^t (I_{PV,out} + I_{BESS} + I_{grid,out} - I_{charging}) dt \quad (16)$$

The  $V_{20}$  is the initial bus voltage of the solar PV MPPT subsystem,  $C_2$  is the DC M.G capacitor value. The solar PV panel MPPT subsystem output current at time  $t$  is  $I_{PV,out}$ , BESS charging and discharging current is  $I_{BESS}$  (or  $I_2$ ) and the final grid current output is  $I_{grid,out}$ . The BESS charging current is given by the equation (17)

$$I_{charging} = \frac{P_{charging}}{V_2\eta_{DC-DC1}} \quad (17)$$

In this, the BESS charging current is determined by the real power flow at the charging terminal through inductance  $L_1$ . the DC M.G voltage is  $V_2$  and the efficiency of the dc to dc bidirectional chopper  $\eta_{DC-DC1}$ . This efficiency depends on the load chopper converter also. The M.G current output  $I_{grid,out}$  is given in equation (18) in terms of the M.G real power  $P_{grid}$ , MG voltage  $V_2$ , and grid boost voltage conversion efficiency  $\eta_{DC-DC2}$ .

$$I_{grid,out} = \frac{P_{grid}}{V_2} \eta_{DC-DC2} \quad (18)$$

The BESS current flow into the M.G is represented in terms of battery voltage  $E$ , the current through the battery cell IBESS with bidirectional dc to dc converter efficiency  $\eta_{DC-DC3}$  is shown in equation (19)

$$I_{BESS,out} = \frac{EI_{BESS}}{V_2} \eta_{DC-DC3} \quad (19)$$

The load voltage  $V_{load}$  or  $V_3$  is given by the buck chopper switching duty cycle  $d_3$  is provided by the equation (20).

$$V_{load} = V_2 \frac{1}{1-d_3} \quad (20)$$

M.G terminal current  $i_{mg}$  gives the dynamic dc link voltage ( $V_{dc}$ ) through the diode  $D_2$  and the bidirectional buck-boost converter with switching duty-cycle  $d_2$  is given by equation (21). The constant  $a=1$  represents boost and  $a=-1$  for buck operation. So, buck and boost operation controlled by the duty cycle  $d_2$  and grid currents.

$$\frac{dV_{dc}}{dt} = a \left( -\frac{i_{mg}}{C_2} + \frac{d_2 i_2}{C_2} \right) \quad (21)$$

The bidirectional buck-boost converter inductor dynamic current flow  $i_{L2}$  is represented using the battery voltage  $E$  and M.G voltage  $V_2$  is given by the equation (22).

$$\frac{di_{L2}}{dt} = a \left( \frac{E}{L_2} - d_2 \frac{V_2}{L_2} \right) \quad (22)$$

The vectorial controlled bidirectional buck-boost converter inductor current represented in terms of M.G capacitor  $C_2$  in terms of transfer function form with the Laplace parameter 's' is given by equation (23)

$$\frac{i_{L2}}{d_2} = \frac{-C_2V_2s - d_2i_{L2}}{C_2L_2s^2 + d_2^2} \quad (23)$$

The M.G terminal voltage-controlled  $V_2$  is done using a current-controlled tuned proportional-integral (P-I) controller is given by the equation (24). Here, the input inductor boost

converter subsystem current reference ( $i_{L1}^*$ ) and actual boost

converter current ( $i_{L1}$ ). The objective of the current P-I controller is maintaining zero or very minimum value between the reference and the actual current value, and ideally, zero is its value.

$$\bar{V}_2 = (i_{L1}^* - i_{L1})(K_{pi} + \frac{1}{K_{ii}s}) \quad (24)$$

The final terminal voltage  $V_2$  and the input solar PV current ( $i_{L1}$ ) are written in the transfer function model with current tuned P-I controller and boost converter duty cycle  $d_1$  is given by the transfer function equation (25)

$$\frac{\bar{V}_2}{i_{L1}^*} = \frac{-K_{pi}K_{ii}d_1V_2s - d_1V_2}{C_2s^3 - C_2V_2K_{pi}K_{ii}s^2 + (d_1^2K_{ii} - C_2V_2)s} \quad (25)$$

*B. Block diagram representation of solar PV system based dc M.G.*

The dc M.G consisting of a solar PV cell system with closed-loop controller representation is shown in Fig.2. The current tuned P-I controller block diagram is  $G_{pi}(s)$ , offset switching frequency ( $G_{sw}(s)$ ), solar PV panel system connected to a dc M.G is  $G_{pv}(s)$  and dc voltage gain function is given by  $A_v(s)$ . The current P-I controller is given by the equation (26) with 's' as the Laplace parameter, current proportionality ( $K_{pi}$ ), and the current integral constant ( $K_{ii}$ ).

$$G_{PI}(s) = K_{pi} + \frac{K_{ii}}{s} \quad (26)$$

The offset switching block ( $G_{sw}(s)$ ) is a relay block that operates based on the reference ( $V_2^*$ ), and actual M.G voltage ( $V_2$ ) is shown in equation (27)

$$G_{sw}(s) = \begin{cases} 1 & V_2 > V_2^* \\ 0 & V_2 < V_2^* \end{cases} \quad (27)$$

The solar PV panel transfer function is considered to be a standard 2nd order function with natural undamped frequency ( $\omega_n$ ), and damping ratio ( $\xi$ ) is given by the equation (28)

$$G_{PV}(s) = \frac{\omega_n^2}{s^2 + 2\xi\omega_n s + \omega_n^2} \quad (28)$$

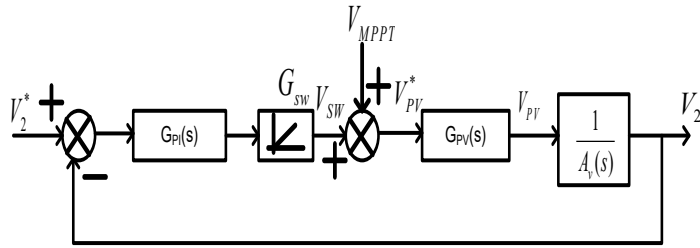


Fig.2. Solar PV microgrid block diagram representation

The dc-dc M.G. voltage gain in BESS switching duty cycle  $d_2$  and solar PV panel inductor  $L_1$  and MG capacitor  $C_2$  is given by the equation (29)

$$A_v(s) = \frac{1 - d_2}{L_1 C_2 s^2 + \frac{L_1}{R_1} s + (1 - d_2)^2} \quad (29)$$

The M.G terminal voltage ( $V_2$ ) with initial voltage  $v_{20}$ , mppt voltage ( $V_{mppt}$ ), output limited transfer function ( $G_{olimit}(s)$ ) and MPPT output transfer function ( $G_{omppt}$ ) is given by the transfer function equation (30)

$$V_2 = G_{olimit}(s)V_{20} - G_{omppt}V_{mppt} \quad (30)$$

And the internal transfer functions for the equation (30) are defined.

The change or error in the M.G terminal voltage is given by the difference between reference and actual M.G voltage, as shown by equation (31). Here, the error in the M.G terminal voltage to zero is the objective.

$$\Delta V_2 = V_2^* - V_2 = \lim_{s \rightarrow 0} s \Delta V_2 = 0 \quad (31)$$

The final output microgrid voltage is represented in the form of a transfer function ( $G_{ov}(s)$ ) in terms of a controller transfer function, solar PV panel transfer function, and dc-dc M.G voltage gain as depicted by equation (32)

$$G_{ov}(s) = G_{PI}(s)G_{PV}(s)\frac{1}{A_v(s)} \quad (32)$$

The ratio of integral to proportional gain constants with a frequency of operation from 5 to 150 Hz is given by (32)

$$\frac{K_{ii}}{K_{pi}} = 2\pi * 100 \quad (32)$$

The final output voltage transfer function is controlled to 1 p.u.(per unit) value as equation (33)

$$|G_{ov}(s)|_{s=j20\pi} = 1 \quad (33)$$

From the equation (32), the open loop output microgrid voltage transfer function based Bode plot and Root-Locus plots are shown for different integral constants in Fig. 3 and Fig.4 the plot parameters has been mentioned in table 1. With increase in the  $K_{ii}$ , the phase margin is moving away from -180 degrees and gain margin is decreasing considerably, thereby stability margin is decreasing. the normal values of  $K_{pp}$  and  $K_{ii}$  are  $1.22e^{-3}$  and 0.77.

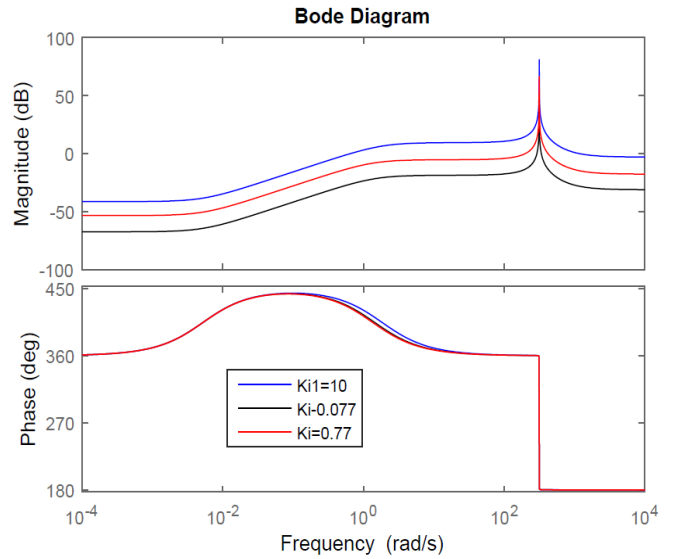


Fig.3. Bode Plot for  $G_{ov}(s)$

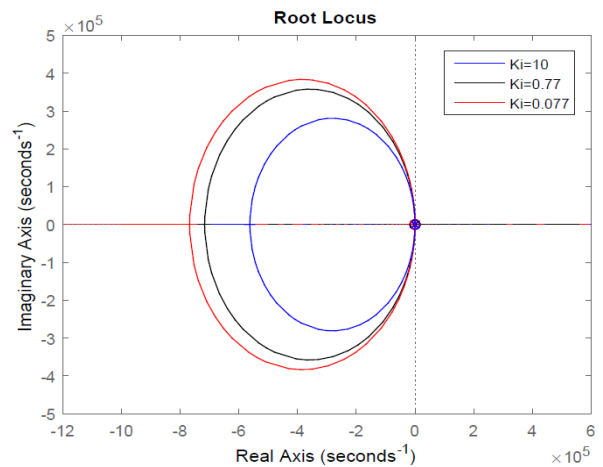


Fig.4. Root-Locus Plot for  $G_{ov}(s)$

TABLE I  
FREQUENCY DOMAIN ANALYSIS

Parameters	Gain Margin	Phase Margin	PM Frequency	Delay Margin	DM Frequency	Stable
Ki=10	1.4084	-110.2359	0.6537	6.6688	0.6537	1
Ki=0.77	35.8508	-179.8441	291.3206	0.0108	291.3206	1
Ki=0.07	7.6823	-179.6415	199.9663	0.0157	199.9663	1

III. TWO AREA-BASED SOLAR PV DC MICROGRID TESTBED SYSTEM

A two-area testbed system interconnected by a shared transmission line network is shown in Fig.5. Each area consists of a small microgrid (M.G) generation system, a BESS, and a solar-PV panel with dc-dc MPPT system tied to a common dc micro-grid with internal loading as shown in Fig.6.

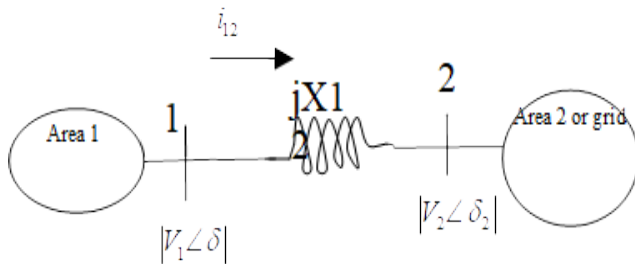


Fig.5. Two area system under study with FACTS devices

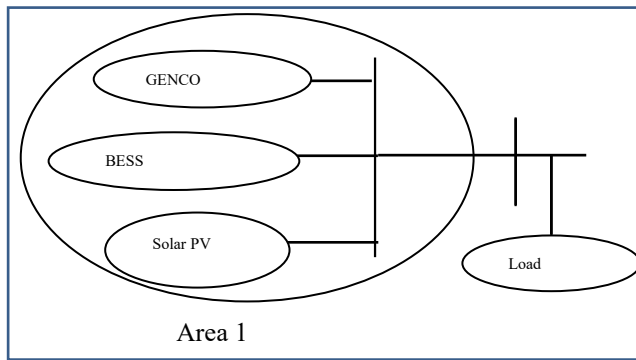


Fig.6. one area source, load schematic

A. Modeling of BESS for solar PV grid-connected system for real power flow sharing

The grid voltage is supposed to be 230V, and the battery converter voltage set at 1.2 times the voltage, which is 276V. If a nominal lithium-ion battery rating of 9V, the number of series battery cells required is  $(270/9)$  31 number. If an Ampere-hour of the battery set to 100, and the power rating for compensation for the solar PV-load system is assumed to be 300KWh, the desired Ah is  $(300K/276)= 1087Ah$  and hence requires  $(1087/100)=11$  cells in parallel. For a voltage source of 276V the Li-ion battery modelling with the equivalent capacitance  $C_b$  is discussed in [35]. To analyse the battery energy storage with the parallel combination of capacitance ( $C_b$ ) and resistance ( $R_b$ ) in series with internal resistance ( $R_{in}$ ) is done using Thevenin's model [35].

B. Solar PV panel closed loop control for maximum real power extraction

The maximum power point tracking (MPPT) technique is generally adopted extract maximum power from the PV cell. The solar PV panel performance will be improved and voltage profile can be maintained at desirable value can be done based on the MPPT technique adopted. There are numerous MPPT techniques available in the literature like Hill climbing etc as discussed in the Section 1. Generally closed loop control schemes are used to track the MPPT for available temperature and irradiance at that erection point. The basic control scheme of the solar PV cell with closed loop transfer function scheme is shown in Fig.7.

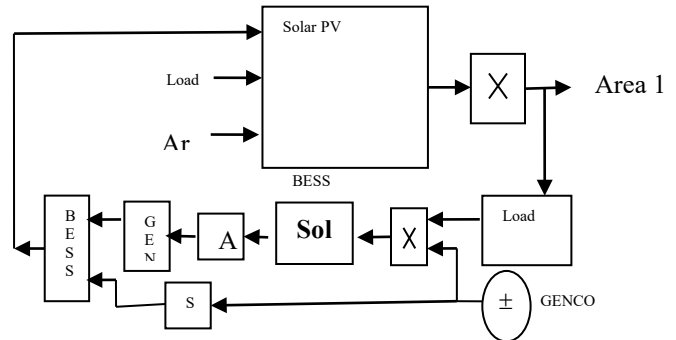


Fig.7 Solar PV closed loop system

The solar PV cell will produce anode voltage ( $V_a$ ) for a natural solar irradiance ( $I_{rad}$ ) and ambient temperature ( $Temp$ ) in degrees at the erection point. The output from solar PV cell is a variable current ( $I_{pv}$ ). When this anode voltage is multiplied with the cell current, output power obtained is ( $P_{pv}$ ). A first order transfer function model will describe the PV cell power depending on the power constants A and K1 as constants. The output from this A, K1 block transfer function is the reference current. The nominal frequency can be (50 or 60Hz) for a 1 volt dc reference per unit (p.u.) voltage ( $V_{ref}$ ). The p.u. voltage is multiplied with this transfer function derived current to extract the reference power value, which is in general the characteristic power of solar PV cell. This power is made optimal so as to achieve the maximum power from the solar cell. To achieve this, one more first order transfer function block with constants B and  $K_2$ . These constants based transfer function is multiplied with a current gain constant C to obtain maximum current extraction value from solar cell.

An integrator in Laplace coefficient S is used to get the area under the curve and to observe its utmost value from the orientation curve. This highest peak voltage ends as added with reference sinusoidal input voltage and meant to the solar PV cell input anode voltage. This basic mechanism assists in two fold. First advantage is to obtain maximum power point (MPP) in the P-V curve and to build it to become stable at this point. Second benefit is to formulate the solar PV cell voltage to maintain unvarying for small variations in the irradiance and temperature. The results for proposed control circuit design is discussed in the next section. The values taken in this paper are  $A=5, B=5.5, C=13.8, D=1/25, K_1=0.5,$  and  $K_2=0.5,$  for a single unit PV panel.

### IV.SOLAR PV WITH MPPT DESIGN WITH METAHEURISTIC-PID (MPID) CONTROL SCHEME

This section discusses MATLAB/Simulink-based design of proportional integral and derivative (PID) Control Scheme. The error in the dc M.G.voltage is the input, and the reference current is the output of the PID controller in this paper. The adaptive P.I.D. Controller with P, I, and D tuning mechanism with initial values adjusted to  $K_{po}$ ,  $K_{do}$ , and  $K_{io}$  are shown in Fig. 8. These sum and initial value blocks are multiplied with respective proportional, derivative and integral weights to get output reference parameter (u). In this paper, the output (u) is the current reference value. The sub-block of  $\text{sum}K_p$ ,  $\text{sum}K_d$ , and  $\text{sum}K_i$  consists of memory block and is shown in Fig.9.

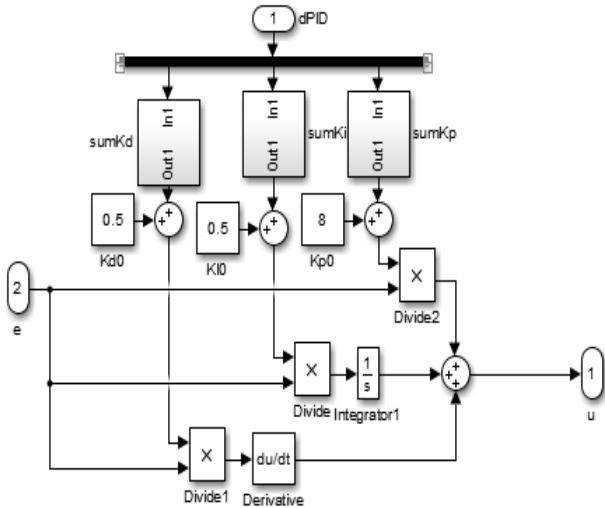


Fig.8. Output sub-block diagram

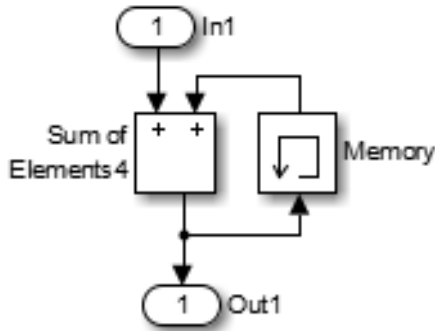


Fig.9. PID error-gain sub-block

The different and most famous metaheuristic techniques like genetic algorithm (GA), particle swarm optimization (PSO), BAT, GWO, improved GA, improved PSO, grasshopper, Ant-Bee Colony, Gravity search, WOA and Pareto search are used for PID tuning and the fitness curve with 500 iterations count is observed as shown in Fig. 10. It is found that GWO and WOA are having very quick fitness curve capability, improved dynamic response, better stability enhancement characteristics among all these metaheuristic algorithms. Hence, we considered to show the GWO and WAO algorithms for oscillations damping and stability improvement in a dc microgrid with solar BESS power network in the next section analyzing about the results. The different few algorithms are

discussed very briefly and complete details will be available in the respective references. This paper used these techniques for the proposed network with PID controller performance enhancement.

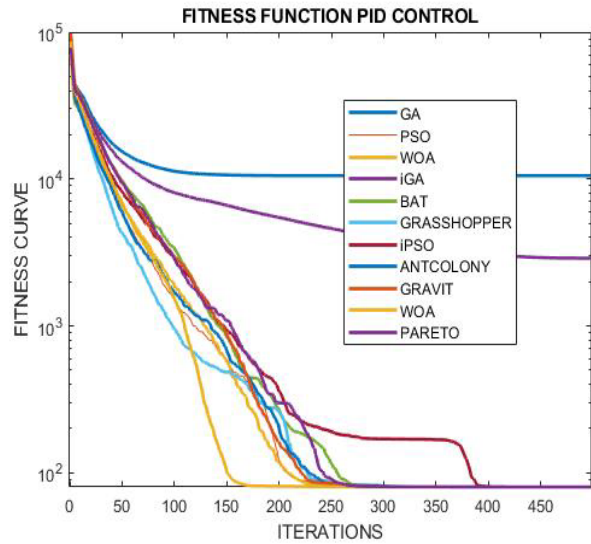


Fig. 10. Fitness curve optimization graphs using various metaheuristic techniques

The multi-objective pseudo code for solar PV MPPT using Gravitational Search Algorithm (GSA) [36 and 37] is shown in algorithm 1.

<b>Algorithm 1:</b>	
<b>Gravitational Search Algorithm (GSA)</b>	
<b>Begin</b>	initialize population and evaluate generation evaluate fitness of agents
<b>while</b>	test for population, mutation until not met; evaluate different directions of total force; calculate velocity and acceleration; repeat while loop
<b>end</b>	
<b>end</b>	

The solar photovoltaic MPPT and stability enhancement using WOA and GWO algorithms(2) and (3) are discussed in [38 and 39]. It is important to mention that A metaheuristic based algorithm (Gravitational search) has been employed in this paper to search and track the maximum power point under various partial shading condition and different parameters change.. A thorough simulation analysis is presented to validate the performance of the algorithm in tracking the optimal power point. Generally, Gravitational search algorithm (GSA) is a swarm intelligence heuristic optimization algorithm based on the law of gravitation. Aiming

at the disadvantage of poor local search ability and slow convergence speed in standard GSA

**Algorithm 2:**  
**Whale Optimization Algorithm (WOA)**

**Begin**  
 initialize population of whales randomly  
 create fitness for search and grading of all the whales  
 test for fitness in population and test further for best search agent (X)

**while**  
 Calculate value of a and other parameters for  $h < 0.5$  and then for  $h > 0.5$   
 different  $|A|$  values, calculate X  
 each search agent  
 repeat till all agents, and positions are checked;  
 update and repeat for all the grading agents or maximum number of populations are achieved;  
 solution with replacement on updated agent solution  
 check for best solution  
 repeat all these steps till all the iterations are checked

**end**  
**end**

**Algorithm 3:**  
**Grey Wolf Optimization Algorithm (GWO)**

**Begin**  
 initialize population of grey wolves, a, A and C  
 evaluate solutions  
 create fitness for search and grading of agents  
 test for fitness in population and test further for first, second and third best solutions

**while**  
 for each search agent  
 update search agent position;  
 repeat till all agents, and positions are checked;  
 update and repeat for all the grading agents or maximum number of populations are achieved;  
 solution with replacement on updated agent solution  
 check for best solution  
 repeat all these steps till all the iterations are checked

**end**  
**end**

V. RESULT ANALYSIS

The solar PV BESS system connected to a dc M.G. with voltage control action using GWO and WAO and without controller response is shown in Fig11 to Fig21. The M.G is started suddenly at 1 second of simulation time, and different parameters' response is analyzed. Based on Fig11, the

solar PV increases output voltage without a controller with time and is said to be unstable when black-started immediately.

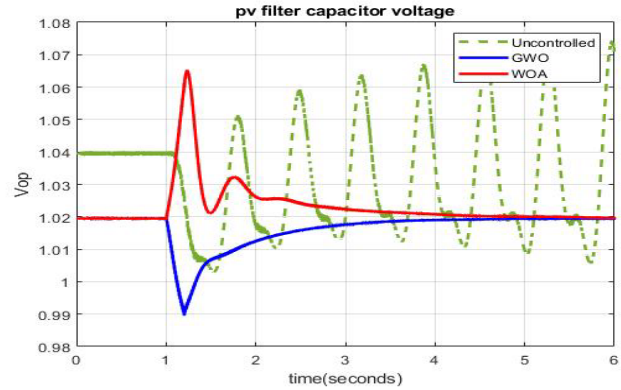


Fig.11. Solar PV output voltage

The solar PV current output after MPPT without a controller, with WAO and GWO, is shown in Fig12. The solar PV current is unstable without a controller.

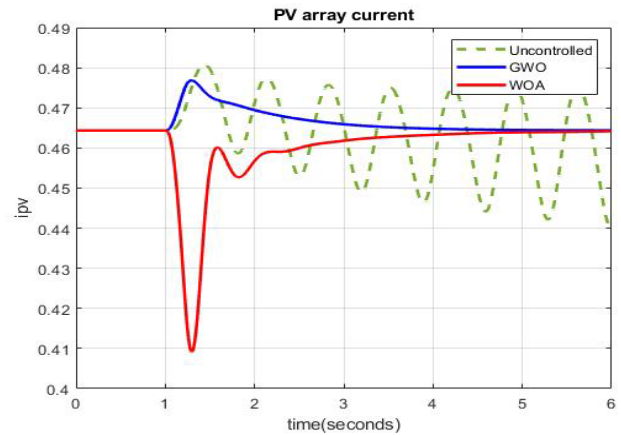


Fig.12. Solar PV current after MPPT

The solar PV panel output current after the inductor filter bank and at the point of M.G connection without a controller, with WAO and GWO, is shown in Fig13. The solar current after the filter bank is having a sustainable operation without a controller with oscillations from 0.65 to 0.2 p.u., range. With FPID, the current surge at 1s black-start.

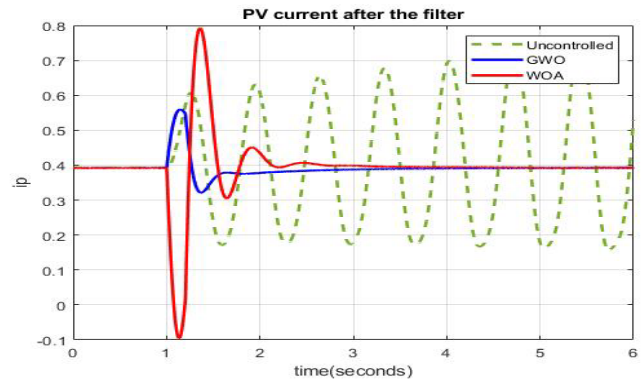


Fig.13. Solar PV current after filter

The solar PV current before the filter without a controller, with WAO and GWO, is shown in Fig14. The current is oscillatory when using the controller. With FPID

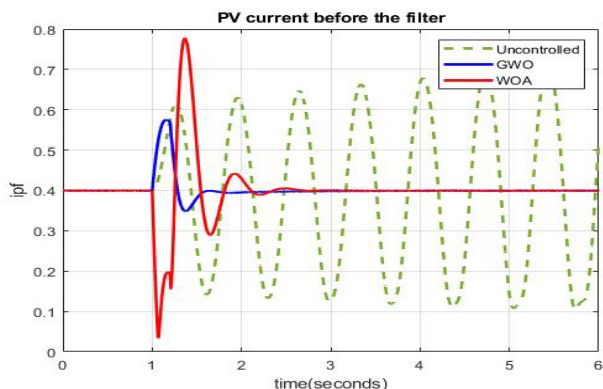


Fig.14. Solar PV current before filter

The voltage at the M.G. terminal ( $V_2$ ) without a controller, with FPID, and with GWO is shown in Fig. 15. The M.G. voltage is unstable when the controller is not used, and the range of oscillations is from 1 to 0.93 p.u, and increasing with time.

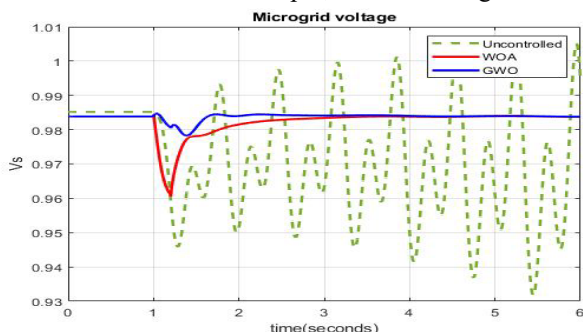


Fig.15. MG injected voltage

The S.G load angle (delta) plot with time in Fig 16. The load angle is unstable without any controller and oscillates between 60 and -40 degrees, increasing exponentially and cosine with time. The WAO and GWO based load angle in degrees increased to 38 and 30 degrees and settled at 2s and 1.5s, respectively, and settled to 20 degrees after that.

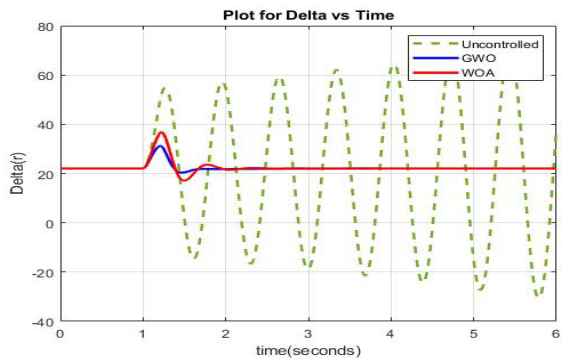


Fig.16.SG power angle (delta)

The d-axis voltage of the S.G. is shown in Fig17. Without a controller, voltage is unstable and increasing oscillatory with a range of 1.5 to 1.1 p.u. With the FPID, this d-axis S.G voltage has two oscillations in the range of 1.3 to 1.2 p.u, and settles at 2.5s to 1.25 p.u. The d-axis voltage with the GWO controller rises to 1.3 p.u, with a single oscillation and settles at 2.5s.

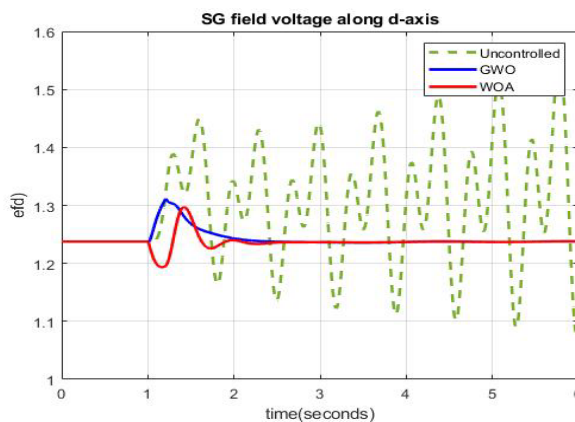


Fig.17. SG d-axis voltage

The BESS terminal voltage without a controller, with WAO and GWO, is shown in Fig. 18.

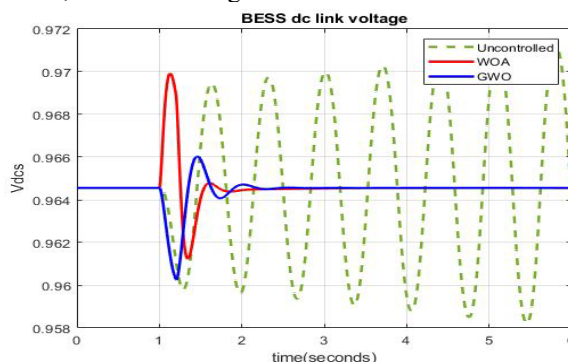


Fig.18. BESS dc link voltage

The S.G. rotor speed without any controller, with WAO and with GWO is shown in Fig. 19. The pace is oscillatory and unstable when not using the controller.

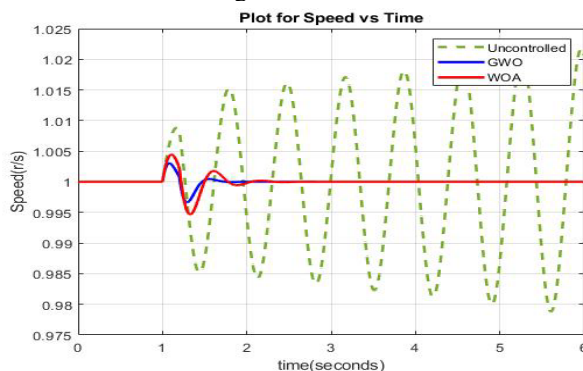


Fig.19. SG rotor speed

The real power injected to the dc M.G by the solar PV BESS system without a controller, FPID, and GWO controller is shown in Fig20. The real power is unstable and oscillatory when using no controller.

The real power injected into the dc M.G. by a P.I controller is 1.774940269747908 p.u, with FPID, 1.79214638652114 p.u GWO, 1.801264409755665p.u. Hence, the active power injection is more with GWO compared to WAO and P.I.D Controller. The elapsed time for the simulation took 25.569193 seconds to complete.

The Results using GWO and WAO without controller response has been shown in table 2

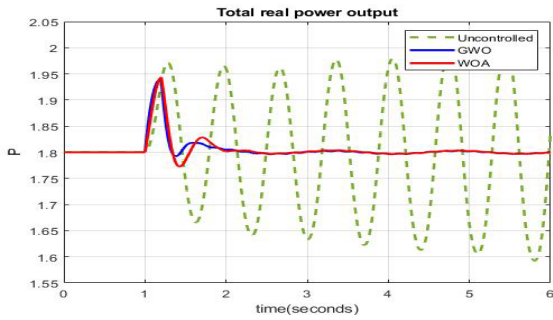


Fig.20. Injected real power

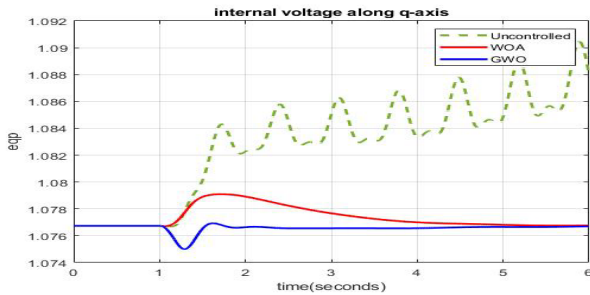


Fig.21. Internal voltage along q-axis supplied to the M.G.

TABLE II  
RESULTS USING GWO AND WAO WITHOUT CONTROLLER RESPONSE

	MG voltage when solar system settles time and value	0.98 p.u at 3sec	0.98 p.u at 1.5sec	oscillations. with GWO
<b>BESS dc link voltage</b>	battery chopper voltage starting	rises to 0.97 p.u., then to 0.96 p.u	rises to 0.97 p.u., then to 0.96 p.u	The GWO is not producing overshoot and results in a smoother and quicker response
	battery chopper voltage settles time and value	settles to 0.965 p.u., at 2.5s	settled at 2s at 0.965 p.u	
<b>SG rotor speed</b>	rotor speed starting	From 1.005 to 0.995 p.u	From 1.003 to 0.998 p.u	Better response with GWO
	rotor speed settles time and value	0.995 p.u at 2sec	Drops at 1.5sec to 1.0 p.u speed value	
<b>Injected real power</b>	Real power injected	Increased to 1.95 p.u then rise to 1.78 p.u	Rise to 1.93p.u then to 1.8 p.u	Better response with GWO
	Real power settles time and value	1.8 p.u at 2.2sec	1.8 at 1.65 sec	

Comparison	Discretion	WAO	GWO	RESULTS
<b>Solar PV output voltage</b>	Solar PV output at (a peak value )	1.065 p.u	0.99 p.u	Better response with GWO
	Solar PV output after 3sec	1.02 p.u	ettles	
<b>Solar PV current after MPPT</b>	Solar current start impulse	0.41 p.u	0.476 p.u	The current surge value is smaller with GWO compared to the WAO value
	Solar current after 3sec	0.465 p.u	settles	
<b>Solar PV current after filter</b>	current surge at 1s black-start	-0.1 to 0.8p.u	0.55	Depicts better settling time, lower peak overshoot, quicker and smoother response with GWO
	Current surge settles time	At 3sec	0.4p.u at 1.5 sec	
<b>Solar PV current before filter</b>	current surges starting at 1s	0 to 0.8 p.u	0.58 p.u	Effective damping with GWO
	Current surge settles time and value	0.4 p.u at 2.5 sec	0.0 p.u at 1.5 sec	
<b>MG injected voltage</b>	MG voltage when solar system start at 1.0p.u	0.98 p.u	0.98 p.u	Smoothly and without

VI.CONCLUSION

The metaheuristic proportional integral and derivative (MPID) controllers with Whale Algorithm Optimization (WAO) Grey Wolf Optimization (GWO) for tuning proportional integral and derivative (PID) for a better power flow control and oscillation damping are discussed in this paper. The synchronous generator (S.G.), solar-PV cell, M.G, and the battery energy storage system (BESS) parameters under the sudden start of the operation are analyzed. The BESS will support solar PV cell power supply under limited process during nights and under shaded conditions. It is observed that without a controller, almost all these device parameters are unstable with increased oscillations. Without the controller, the system cannot sustain a constant grid voltage or rotor speed and resulted in sustained fluctuations in PV voltage, current, power angle (delta), rotor speed, and BESS terminal voltage. The same device values are damped effectively and reached a steady reference value when WAO or GWO controller is used for the same system. Compared to WAO, the GWO results in decreased peak overshoot, smoother settling, lesser oscillations, and better settling time. The GWO running time is quicker in response and has better adaptability with almost all the parameter independent compared to the WAO controller. The real power injection is more with GWO compared to the WAO controller. Hence, the GWO controller-based dc M.G, system is parameter independent and has a robust and effective performance than the WAO controller.

## REFERENCES

- [1] Tie, Siang Fui, and Chee Wei Tan. "A review of energy sources and energy management system in electric vehicles." *Renewable and sustainable energy reviews* 20 (2013): 82-102.
- [2] Rauschenbach, Hans S. *Solar cell array design handbook: the principles and technology of photovoltaic energy conversion*. Springer science & business media, 2012.
- [3] Li, Quan, and Peter Wolfs. "A review of the single phase photovoltaic module integrated converter topologies with three different D.C. link configurations." *IEEE Transactions on power electronics* 23, no. 3 (2008): 1320-1333.
- [4] Hafiz, Faeza, Anderson Rodrigo de Queiroz, and Iqbal Husain. "Multi-stage stochastic optimization for a PV-storage hybrid unit in a household." In *2017 IEEE Industry Applications Society Annual Meeting*, pp. 1-7. IEEE, 2017.
- [5] Gouda, Eid Abdelbaki, Ahmed Abd-Alaziz, and Magdi El-Saadawi. "Design modeling, and control of multi-stage SMES integrated with P.V. system." *Journal of Energy Storage* 29 (2020): 101399.
- [6] Hu, Yihua, Wenping Cao, Bing Ji, Jikai Si, and Xiangping Chen. "New multi-stage D.C.-D.C. converters for grid-connected photovoltaic systems." *Renewable energy* 74 (2015): 247-254.
- [7] Chaurasiya, Prem Kumar, Vilas Warudkar, and Siraj Ahmed. "Wind energy development and policy in India: A review." *Energy Strategy Reviews* 24 (2019): 342-357.
- [8] <https://www.worldenergy.org/data/resources/resource/solar/>.
- [9] El-Shahat, Adel, and Sharaf Sumaiya. "DC-microgrid system design, control, and analysis." *Electronics* 8, no. 2 (2019): 124.
- [10] Nansur, Ainur Rofiq, Alfis Syah Laili Hermawan, and Farid Dwi Mudiarto. "Constant voltage control using fuzzy logic controller (FLC) to overcome the unstable output voltage of MPPT in DC microgrid system." In *2018 International Electronics Symposium on Engineering Technology and Applications (IES-ETA)*, pp. 19-24. IEEE, 2018.
- [11] Vasantharaj, Subramanian, Vairavasundaram Indragandhi, Vairavasundaram Subramaniaswamy, Yuvaraja Teekaraman, Ramya Kuppusamy, and Srete Nikolovski. "Efficient Control of DC Microgrid with Hybrid PV—Fuel Cell and Energy Storage Systems." *Energies* 14, no. 11 (2021): 3234.
- [12] Yan, Hein Wai, Glen G. Farivar, Neha Beniwal, Naga Brahmendra Yadav Gorla, Hossein Dehghani Tafti, Salvador Ceballos, Josep Pou, and Georgios Konstantinou. "Control strategy for effective battery utilization in a stand-alone dc microgrid with solar energy." In *2021 IEEE Energy Conversion Congress and Exposition (ECCE)*, pp. 1046-1051. IEEE, 2021.
- [13] Satapathy, Manoranjan, Meher Preetam Korukonda, Amir Hussain, and Laxmidhar Behera. "A direct perturbation based sensor-free mppt with dc bus voltage control for a standalone dc microgrid." In *2019 IEEE PES Innovative Smart Grid Technologies Europe (ISGT-Europe)*, pp. 1-5. IEEE, 2019.
- [14] Das, Saborni, Abhik Hazra, and Mousumi Basu. "Metaheuristic optimization based fault diagnosis strategy for solar photovoltaic systems under non-uniform irradiance." *Renewable energy* 118 (2018): 452-467.
- [15] Pathak, Pawan Kumar, Anil Kumar Yadav, and P. A. Alvi. "A state-of-the-art review on shading mitigation techniques in solar photovoltaics via meta-heuristic approach." *Neural Computing and Applications* (2021): 1-39.
- [16] Bodha, Kapil Deo, Vinod Kumar Yadav, and Vivekananda Mukherjee. "A novel quantum inspired hybrid metaheuristic for dispatch of power system including solar photovoltaic generation." *Energy Sources, Part B: Economics, Planning, and Policy* 16, no. 6 (2021): 558-583.
- [17] Pillai, Dhanup S., and N. Rajasekar. "Metaheuristic algorithms for PV parameter identification: A comprehensive review with an application to threshold setting for fault detection in PV systems." *Renewable and Sustainable Energy Reviews* 82 (2018): 3503-3525.
- [18] Mohamed, Mohamed A., Ahmed A. Zaki Diab, and Hegazy Rezk. "Partial shading mitigation of PV systems via different metaheuristic techniques." *Renewable energy* 130 (2019): 1159-1175.
- [19] Das, Monotosh, Maisanam Anil Kumar Singh, and Agnimitra Biswas. "Techno-economic optimization of an off-grid hybrid renewable energy system using metaheuristic optimization approaches—case of a radio transmitter station in India." *Energy conversion and management* 185 (2019): 339-352.
- [20] Sun, Jiwei, Wei Lin, Mingguo Hong, and Kenneth A. Loparo. "Voltage Regulation of DC-microgrid with P.V. and Battery." *IEEE Transactions on Smart Grid* 11, no. 6 (2020): 4662-4675.
- [21] Gu, Yunjie, Wuhua Li, and Xiangning He. "Passivity-based control of D.C. microgrid for self-disciplined stabilization." *IEEE Transactions on Power Systems* 30, no. 5 (2014): 2623-2632.
- [22] Doshi, Karan, and V. S. K. V. Harish. "Analysis of a wind-PV battery hybrid renewable energy system for a dc microgrid." *Materials Today: Proceedings* (2020).
- [23] Alam, Mohd, Kuldeep Kumar, Saket Verma, and Viresh Dutta. "Renewable sources based D.C. microgrid using hydrogen energy storage: Modelling and experimental analysis." *Sustainable Energy Technologies and Assessments* 42 (2020): 100840.
- [24] Wang, Shuoqi, Languang Lu, Xuebing Han, Minggao Ouyang, and Xuning Feng. "Virtual-battery based droop control and energy storage system size optimization of a D.C. microgrid for electric vehicle fast charging station." *Applied Energy* 259 (2020): 114146.
- [25] Han, Ying, Hanqing Yang, Qi Li, Weirong Chen, Firuz Zare, and Josep M. Guerrero. "Mode-triggered droop method for the decentralized energy management of an islanded hybrid P.V./hydrogen/battery D.C. microgrid." *Energy* 199 (2020): 117441.
- [26] Matayoshi, Hidehito, Mitsunaga Kinjo, Shiram S. Rangarajan, Girish Ganesan Ramanathan, Ashraf M. Hemeida, and Tomonobu Senjyu. "Islanding operation scheme for D.C. microgrid utilizing pseudo Droop control of photovoltaic system." *Energy for Sustainable Development* 55 (2020): 95-104.
- [27] Singh, Prashant, and J. S. Lather. "Dynamic current sharing, voltage and S.O.C. regulation for HESS based D.C. microgrid using CPISM technique." *Journal of Energy Storage* 30 (2020): 101509.
- [28] Singh, Prashant, and J. S. Lather. "Dynamic current sharing, voltage and S.O.C. regulation for HESS based D.C. microgrid using CPISM technique." *Journal of Energy Storage* 30 (2020): 101509.
- [29] Naik, Jyotirmayee, Snehamoy Dhar, and P. K. Dash. "Adaptive differential relay coordination for PV DC microgrid using a new kernel based time-frequency transform." *International Journal of Electrical Power & Energy Systems* 106 (2019): 56-67.
- [30] Armghan, Hammad, Ming Yang, M. Q. Wang, Naghmash Ali, and Ammar Armghan. "Nonlinear integral backstepping based control of a D.C. microgrid with renewable generation and energy storage systems." *International Journal of Electrical Power & Energy Systems* 117 (2020): 105613.
- [31] Nguyen, Duy-Long, and Hong-Hee Lee. "Fuzzy P.I.D. Controller for Adaptive Current Sharing of Energy Storage System in D.C. Microgrid." In *International Conference on Intelligent Computing*, pp. 213-223. Springer, Cham, 2020.
- [32] Al-Sakkaf, Shehab, Mahmoud Kassas, Muhammad Khalid, and Mohammad A. Abido. "An energy management system for residential autonomous D.C. microgrid using optimized fuzzy logic controller considering economic dispatch." *Energies* 12, no. 8 (2019): 1457.
- [33] Sun, Qian, Qiuye Sun, and Dehao Qin. "Adaptive fuzzy droop control for optimized power sharing in an islanded microgrid." *Energies* 12, no. 1 (2019): 45.
- [34] Ananth, D., G. N. Kumar, D. Deepak Chowdary, and K. Appala Naidu. "Damping of Power System Oscillations and Control of Voltage Dip by Using STATCOM and UPFC." *International Journal of Pure and Applied Mathematics* 114, no. 10 (2017): 487-496.
- [35] Gayathri, T., D. V. N. Ananth, GV Nagesh Kumar, and G. Sivanagaraju. "Enhancement in dynamic and LVRT behaviour of an EFOC controlled DFIG with integrated Battery Energy Storage System." In *2013 Annual IEEE India Conference (INDICON)*, pp. 1-6. IEEE, 2013.
- [36] Pani, Alok Kumar, and Niranjana Nayak. "Forecasting solar irradiance with weather classification and chaotic gravitational search algorithm based wavelet kernel extreme learning machine." *International Journal of Renewable Energy Research (IJRER)* 9, no. 4 (2019): 1650-1659.
- [37] Li, Ling-Ling, Guo-Qian Lin, Ming-Lang Tseng, Kimhua Tan, and Ming K. Lim. "A maximum power point tracking method for PV

- system with improved gravitational search algorithm." *Applied Soft Computing* 65 (2018): 333-348.
- [38] Xiong, Guojiang, Jing Zhang, Dongyuan Shi, and Yu He. "Parameter extraction of solar photovoltaic models using an improved whale optimization algorithm." *Energy conversion and management* 174 (2018): 388-405.
- [39] Chawla, V., A. Chanda, and S. Angra. "Automatic guided vehicles fleet size optimization for flexible manufacturing system by grey wolf optimization algorithm." *Management Science Letters* 8, no. 2 (2018): 79-90.